

# Doubly Stochastic Subspace Clustering

Derek Lim

Department of Computer Science  
Cornell University  
dl772@cornell.edu

René Vidal

Mathematical Institute for Data Science  
Johns Hopkins University  
{rvidal, bhaeffele}@jhu.edu

Benjamin D. Haeffele

## Abstract

Many state-of-the-art subspace clustering methods follow a two-step process by first constructing an affinity matrix between data points and then applying spectral clustering to this affinity. Most of the research into these methods focuses on the first step of generating the affinity matrix, which often exploits the self-expressive property of linear subspaces, with little consideration typically given to the spectral clustering step that produces the final clustering. Moreover, existing methods obtain the affinity by applying ad-hoc postprocessing steps to the self-expressive representation of the data, and this postprocessing can have a significant impact on the subsequent spectral clustering step. In this work, we propose to unify these two steps by jointly learning both a self-expressive representation of the data and an affinity matrix that is well-normalized for spectral clustering. In the proposed model, we constrain the affinity matrix to be doubly stochastic, which results in a principled method for affinity matrix normalization while also exploiting the known benefits of doubly stochastic normalization in spectral clustering. While our proposed model is non-convex, we give a convex relaxation that is provably equivalent in many regimes; we also develop an efficient approximation to the full model that works well in practice. Experiments show that our method achieves state-of-the-art subspace clustering performance on many common datasets in computer vision.

## 1. Introduction

Subspace clustering seeks to cluster a set of data points that are approximately drawn from a union of low dimensional linear (or affine) subspaces into clusters, where each linear (or affine) subspace defines a cluster (i.e., every point in a given cluster lies in the same subspace) [34]. The most common class of subspace clustering algorithms for clustering a set of  $n$  datapoints are those that proceed in two stages: 1) Learning an affinity matrix  $\mathbf{A} \in \mathbb{R}^{n \times n}$  that defines the similarity between pairs of datapoints; 2) Applying a graph

clustering technique, such as spectral clustering [36, 32], to produce the final clustering. Within this general framework, a large majority of research into subspace clustering methods has largely focused on how to construct the affinity matrix, with relatively little attention given to the subsequent spectral clustering step. In particular, arguably the most popular model for subspace clustering is to construct the affinity matrix by exploiting the ‘self-expressive’ property of linear (or affine) subspaces, where a point within a given subspace can be represented as a linear combination of other points within the subspace [7, 8, 25, 43, 44, 34]. For a dataset  $\mathbf{X} \in \mathbb{R}^{d \times n}$  of  $n$ ,  $d$ -dimensional points, this is typically captured by an optimization problem of the form:

$$\min_{\mathbf{C}} \frac{1}{2} \|\mathbf{X} - \mathbf{XC}\|_F^2 + \lambda\theta(\mathbf{C}), \quad (1)$$

where the first term captures the self-expressive property,  $\mathbf{X} \approx \mathbf{XC}$ , and the second term,  $\theta$ , is some regularization term on  $\mathbf{C}$  to encourage that a given point is primarily represented by other points from its own subspace and to avoid trivial solutions such as  $\mathbf{C} = \mathbf{I}$ . Once the self-expressive representation  $\mathbf{C}$  has been learned from (1), the final affinity  $\mathbf{A}$  is then typically constructed by rectifying and symmetrizing  $\mathbf{C}$ , e.g.,  $\mathbf{A} = (|\mathbf{C}| + |\mathbf{C}^\top|)/2$ .

However, as we detail in Section 2.1, many subspace clustering methods require ad-hoc or unjustified postprocessing procedures on  $\mathbf{C}$  to work in practice; this is illustrated in Figure 1. These postprocessing steps serve to normalize  $\mathbf{C}$  to produce an affinity  $\mathbf{A}$  with better spectral clustering performance, but they add numerous arbitrary hyperparameters to the models and receive little mention in the associated papers. Likewise, it is well-established that some form of Laplacian normalization is needed for spectral clustering to be successful, for which the practitioner again has multiple choices of normalization strategy.

In this paper, we propose a new subspace clustering framework which explicitly connects the self-expressive step, the affinity normalization, and the spectral clustering step. To motivate our proposed model, we first discuss the desired properties of subspace clustering affinities one would like for successful spectral clustering. Specifically,

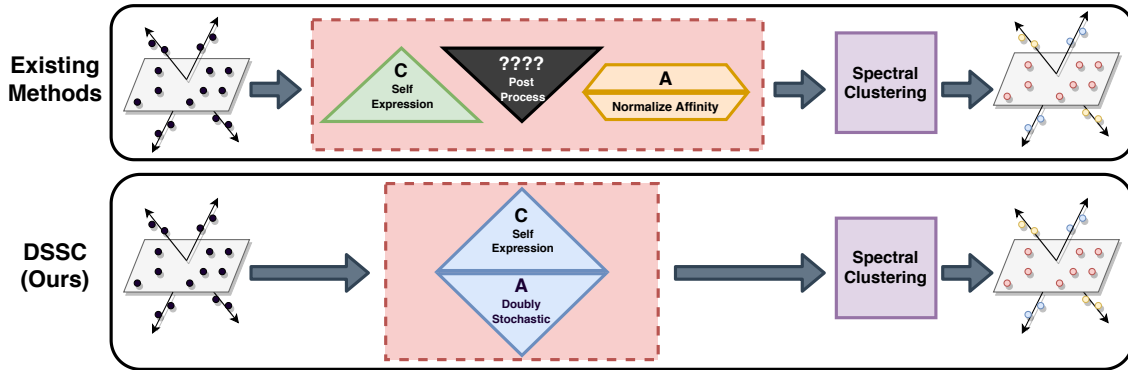


Figure 1. Diagram comparing our DSSC framework with existing methods for self-expressive affinity-based subspace clustering. (Top row) Most existing methods focus on computing the self-expressive matrix  $\mathbf{C}$ , but they are also reliant on choices of postprocessing and affinity normalization, which often take the form of ad-hoc procedures that are not well-studied. (Bottom row) Our DSSC models learn a doubly stochastic affinity matrix  $\mathbf{A} \in \Omega_n$  along with the self-expressive matrix  $\mathbf{C}$ . The doubly stochastic affinity does not require postprocessing or normalization to be used for spectral clustering and has numerous desirable properties for subspace clustering.

we desire affinities  $\mathbf{A}$  that have the following properties:

- (A1) *Well-normalized for spectral clustering.* We should better leverage knowledge that  $\mathbf{A}$  will be input to spectral clustering. Many forms of ad-hoc postprocessing in subspace clustering perform poorly-justified normalization, and there is also a choice of normalization to be made in forming the graph Laplacian [36].
- (C1) *Sparsity.* Much success in subspace clustering has been found with enforcing sparsity on  $\mathbf{C}$  [7, 8, 44]. In particular, many sparsity-enforcing methods are designed to ensure that the nonzero entries of the affinity matrix correspond to pairs of points which belong to the same subspace. This leads to high clustering accuracy, desirable computational properties, and provable theoretical guarantees.
- (C2) *Connectivity.* There should be sufficiently many edges in the underlying graph of  $\mathbf{A}$  so that all points within the same subspace are connected [27, 40, 43]. Thus, there is a trade-off between sparsity and connectivity that subspace clustering methods must account for.

Properties (C1) and (C2) are well studied in the subspace clustering literature, and can be enforced on the self-expressive  $\mathbf{C}$ , since rectifying and symmetrizing a  $\mathbf{C}$  with these properties, for example, maintains these properties. However, property (A1) must be enforced on  $\mathbf{A}$ , so it is often neglected in several aspects and mostly handled by ad-hoc postprocessing methods, if handled at all. In working towards (A1), we first constrain  $\mathbf{A} \geq \mathbf{0}$ , since nonnegativity of the affinity is necessary for interpretability and alignment with spectral clustering theory. Beyond this, spectral clustering also benefits from having rows and columns in the affinity matrix of the same scale; several subspace clustering algorithms postprocess the self-expressive  $\mathbf{C}$  by normalizing the columns of  $\mathbf{C}$  before forming an affinity, and many forms of Laplacian normalization for spectral

clustering normalize rows and/or columns to have similar scale [36]. In particular, one form of normalization which is well established in the spectral clustering literature is to constrain the rows and columns to have unit  $l_1$  norm. Because  $\mathbf{A}$  is additionally constrained to be nonnegative, this is equivalent to requiring each row sum and column sum of  $\mathbf{A}$  to be 1, resulting in constraints that restrict the affinities  $\mathbf{A}$  to be in the convex set of doubly stochastic matrices [14]:

$$\Omega_n = \{\mathbf{A} \in \mathbb{R}^{n \times n} \mid \mathbf{A} \geq \mathbf{0}, \mathbf{A}\mathbf{1} = \mathbf{1}, \mathbf{A}^\top \mathbf{1} = \mathbf{1}\}. \quad (2)$$

Doubly stochastic matrices have been thoroughly studied for spectral clustering, and doubly stochastic normalization has been shown to significantly improve the performance of spectral clustering [45, 46, 39, 29, 12, 15, 37, 19]. Moreover, doubly stochastic matrices are invariant to the most widely-used types of Laplacian normalization [36], which removes the need to choose a Laplacian normalization scheme. Further, the authors of [46] show that various Laplacian normalization schemes can be viewed as attempting to approximate a given affinity matrix with a doubly stochastic matrix under certain distance metrics.

Beyond being well-normalized for spectral clustering (A1), the family of doubly stochastic matrices can also satisfy properties (C1) and (C2). Our proposed methods will give control over the sparsity-connectivity trade-off through interpretable parameters, and we in practice learn  $\mathbf{A}$  that are quite sparse. Additionally, doubly stochastic matrices have a guarantee of a certain level of connectivity due to the row sum constraint, which prohibits solutions with all-zero rows (that can occur in other subspace clustering methods).

**Contributions.** In this work, we develop a framework that unifies the self-expressive representation step of subspace clustering with the spectral clustering step by formulating a model that jointly solves for a self-expressive representation  $\mathbf{C}$  and a doubly stochastic affinity matrix  $\mathbf{A}$ . While our pro-

posed model is non-convex, we provide a convex relaxation; we show theoretically that this relaxation is exactly equivalent to the original model in most relevant regimes and gives close approximations to the non-convex model in all other regimes. We additionally develop an efficient algorithm based on linearized ADMM [26] to compute the solution to our convex model. A closer analysis of our model allows us to formulate an alternative algorithm to quickly compute an approximate solution, in which we first efficiently learn a self-expressive matrix and then subsequently fit a doubly stochastic matrix by a regularized optimal transport problem [2, 23]. This approximate model further has interpretations as a principled postprocessing for a wide class of subspace clustering algorithms. Finally, we validate our approach with experiments on various standard subspace clustering datasets, where we demonstrate that our models significantly improve on the current state-of-the-art in a variety of performance metrics.

### 1.1. Related Work

We review several methods that attempt to integrate the self-expressive step with the final clustering or that explore regularization similar to a doubly stochastic constraint. Structured SSC [20] seeks to connect the self-expressive affinity learning step with the spectral clustering step. It formulates an optimization problem in which a self-expressive affinity and a spectral-clustering-related matrix is learned, but they constrain their clustering matrix to be a binary matrix — thus making their formulation non-convex and requiring a full spectral clustering step in each iteration of their optimization algorithm. In contrast, our method only constrains the clustering matrix to be doubly stochastic, thus maintaining a convex formulation and only requiring a single spectral clustering at the end.

There has also been work in sparse representation that processes a dissimilarity matrix (that can be viewed as the complement of a corresponding affinity matrix) to learn a sparse row stochastic representation matrix [6, 5]. These works are mostly different in focus, as they seek to find representatives for the data and do not use spectral clustering in downstream tasks.

Scaled Simplex SSC learns a scaled column stochastic matrix [42], but it only allows representation with nonnegative coefficients. This and other subspace clustering methods that learn nonnegative self-expressive coefficients like SSQP [38] fail in certain cases. They tend to only connect points with positive correlation to each other, even though points in the same subspace can have very negative correlation (e.g.  $\mathbf{x}$  and  $-\mathbf{x} \in \mathbb{R}^d$  are in the same subspace).

While no subspace clustering methods consider learning doubly stochastic affinities, the use of doubly stochastic affinities is well-established in spectral clustering. In particular, Zass and Shashua find strong performance by ap-

plying spectral clustering to the nearest doubly stochastic matrix to the input affinity in Frobenius norm [46]. Also, there has been work on learning doubly stochastic approximations of input affinity matrix subject to rank constraints [29, 39]. Further, if one forms the affinity matrix using a Gaussian kernel, which is often done in spectral clustering, Landa *et al.* show that doubly stochastic normalization of the kernel matrix by diagonal matrix scaling is robust to heteroskedastic additive noise on the data points [19].

## 2. Doubly Stochastic Models

In this section, we further detail the motivation for learning doubly stochastic affinities for subspace clustering. Then we develop two models for subspace clustering with doubly stochastic affinities. Our J-DSSC model provides a formulation for jointly learning a self-expressive matrix and doubly stochastic affinity, while our A-DSSC model is a fast approximation that sequentially solves for a self-expressive matrix and then a doubly stochastic affinity that approximates it.

### 2.1. Benefits of Doubly Stochastic Affinities

As discussed above, existing subspace clustering methods such as SSC [8], LRR [22], EDSC [16], EnSC [43], and deep subspace clustering networks (DSC-Net) [17] require various ad-hoc postprocessing methods to achieve strong clustering performance on certain datasets. For example, it has recently been shown experimentally that if one removes the ad-hoc postprocessing step from DSC-Net [17] then the performance drops considerably — performing no better than simple baseline methods and far below state-of-the-art [11]. Common postprocessing steps include keeping only the top  $l$  entries of each column of  $\mathbf{C}$ , normalizing columns of  $\mathbf{C}$ , and/or using SVD-based postprocessing, each of which introduces extra hyperparameters and degrees of freedom for the practitioner. Likewise, the practitioner is also required to make a choice on the particular type of Laplacian normalization to use [36].

To better connect the self-expressive step with the subsequent spectral clustering step and to avoid the need for ad-hoc postprocessing methods, we propose a framework for directly learning an affinity  $\mathbf{A}$  that already has desired properties (A1) and (C1)-(C2) for spectral clustering. Restricting  $\mathbf{A} \in \Omega_n$  to be doubly stochastic achieves these goals. While a wide variety of regularization types and affinity constraints have been used in self-expressive subspace clustering methods [24], doubly stochastic constraints have not been leveraged.

As noted in the introduction, doubly stochastic matrices are already nonnegative, so we do not need to take absolute values of some computed matrix. Also, each row and column of a doubly stochastic matrix sums to one, so they each have the same scale in  $l_1$  norm — removing the need

to postprocess by scaling rows or columns. Importantly for (A1), doubly stochastic matrices are also invariant to most forms of Laplacian normalization used in spectral clustering. For example, for a symmetric affinity matrix  $\mathbf{A}$  with row sums  $\mathbf{D} = \text{diag}(\mathbf{A}\mathbf{1})$ , widely used Laplacian variants include the unnormalized Laplacian  $\mathbf{D} - \mathbf{A}$ , the normalized Laplacian  $\mathbf{I} - \mathbf{D}^{-1/2}\mathbf{A}\mathbf{D}^{-1/2}$ , and the random walk Laplacian  $\mathbf{I} - \mathbf{D}^{-1}\mathbf{A}$  [36]. When  $\mathbf{A}$  is doubly stochastic, the matrix of row sums satisfies  $\mathbf{D} = \mathbf{I}$ , so all of the normalization variants are equivalent and give the same Laplacian  $\mathbf{I} - \mathbf{A}$ .

In addition, many types of regularization and constraints that have been proposed for subspace clustering tend to desire sparsity (C1) and connectivity (C2), in the sense that they want  $\mathbf{A}_{ij}$  to be small in magnitude or zero when  $\mathbf{x}_i$  and  $\mathbf{x}_j$  belong to different subspaces and to be nonzero for sufficiently many pairs  $(i, j)$  where  $\mathbf{x}_i$  and  $\mathbf{x}_j$  belong to the same subspace [27, 40]. The doubly stochastic matrices learned by our models can be tuned to achieve any desired sparsity level. Also, doubly stochastic affinities are guaranteed a certain level of connectedness, as each row must sum to 1. This means that there cannot be any zero rows in the learned affinity, unlike in methods that compute representations one column at a time such as SSC [8], EnSC [43], and SSC-OMP [44], where it is possible that a point is never used in the self-expressive representation of other points.

## 2.2. Joint Learning: J-DSSC

In developing our model to jointly learn a self-expressive matrix and doubly stochastic affinity, we build off of the general regularized self-expression form in (1). In particular, in addition to learning a self-expressive matrix  $\mathbf{C}$  we also wish to learn a doubly stochastic affinity matrix  $\mathbf{A} \in \Omega_n$ . Now, note that self-expressive models (roughly) model  $|\mathbf{C}_{ij}|$  as proportional to the likelihood that  $x_i$  and  $x_j$  are in the same subspace, so we desire that our normalized affinity,  $\mathbf{A}$ , be close to  $|\mathbf{C}|$  (optionally after scaling  $\mathbf{A}$  by a constant to match the scale of  $|\mathbf{C}|$ ), which we incorporate via the use of a penalty function  $\Theta(\cdot, \cdot)$ . Thus, we have a general framework:

$$\begin{aligned} \min_{\mathbf{C}, \mathbf{A}} \frac{1}{2} \|\mathbf{X} - \mathbf{X}\mathbf{C}\|_F^2 + \lambda\theta(\mathbf{C}) + \gamma\Theta(|\mathbf{C}|, \mu\mathbf{A}) \\ \text{s.t. } \mathbf{A} \in \Omega_n, \text{diag}(\mathbf{C}) = \mathbf{0} \end{aligned} \quad (3)$$

The zero-diagonal constraint on  $\mathbf{C}$  is enforced to prevent each point from using itself in its self-representation, as this is not informative for clustering. For our particular choice of  $\Theta$ , we use an  $l_2$  distance penalty, as  $l_2$  projection of an affinity matrix onto the doubly stochastic matrices often improves spectral clustering performance [46] and results in desirable sparsity properties [31, 2]. As a result, our proposed model takes the form of an optimization problem over

$\mathbf{C}$  and  $\mathbf{A}$ :

$$\begin{aligned} \min_{\mathbf{C}, \mathbf{A}} \frac{1}{2} \|\mathbf{X} - \mathbf{X}\mathbf{C}\|_F^2 + \frac{\eta_1}{2} \|\mathbf{C}\|_F^2 + \eta_2 \|\mathbf{C} - \eta_2\mathbf{A}\|_F^2 + \eta_3 \|\mathbf{C}\|_1 \\ \text{s.t. } \mathbf{A} \in \Omega_n, \text{diag}(\mathbf{C}) = \mathbf{0}, \end{aligned} \quad (4)$$

where  $\eta_1, \eta_2 > 0, \eta_3 \geq 0$  are hyperparameters.

The objective (4) is not convex because of the  $|\mathbf{C}|$  term in the  $\mathbf{C}$ -to- $\mathbf{A}$ -difference loss. To alleviate this issue, we relax the problem by separating the self-expressive matrix  $\mathbf{C}$  into two nonnegative matrices  $\mathbf{C}_p, \mathbf{C}_n \geq \mathbf{0}$ , so that  $\mathbf{C}_p - \mathbf{C}_n$  takes the role of  $\mathbf{C}$  and  $\mathbf{C}_p + \mathbf{C}_n$  approximately takes the role of  $|\mathbf{C}|$  (with the approximation being exact if the nonzero support of  $\mathbf{C}_p$  and  $\mathbf{C}_n$  do not overlap). Thus, our convex model is given by:

$$\begin{aligned} \min_{\mathbf{C}_p, \mathbf{C}_n, \mathbf{A}} \frac{1}{2} \|\mathbf{X} - \mathbf{X}[\mathbf{C}_p - \mathbf{C}_n]\|_F^2 + \\ \frac{\eta_1}{2} \|[\mathbf{C}_p + \mathbf{C}_n] - \eta_2\mathbf{A}\|_F^2 + \eta_3 \|\mathbf{C}_p + \mathbf{C}_n\|_1 \\ \text{s.t. } \mathbf{A} \in \Omega_n, \mathbf{C}_p, \mathbf{C}_n \in \mathbb{R}_{\geq 0, \text{diag}=\mathbf{0}}^{n \times n} \end{aligned} \quad (5)$$

where  $\mathbb{R}_{\geq 0, \text{diag}=\mathbf{0}}^{n \times n}$  is the set of  $n \times n$  real matrices with nonnegative entries and zero diagonal<sup>1</sup>. This problem is now convex and can be efficiently solved to global optimality, as we show in Section 3.1. We refer to this model as Joint Doubly Stochastic Subspace Clustering (J-DSSC).

If the optimal  $\mathbf{C}_p$  and  $\mathbf{C}_n$  have disjoint support (where the support of a matrix is the set of indices  $(i, j)$  where the matrix is nonzero), then by solving (5) we also obtain a solution for (4), since we can take  $\mathbf{C} = \mathbf{C}_p - \mathbf{C}_n$ , in which case  $|\mathbf{C}| = |\mathbf{C}_p - \mathbf{C}_n| = \mathbf{C}_p + \mathbf{C}_n$ . However, this final equality does not hold when the optimal  $\mathbf{C}_p$  and  $\mathbf{C}_n$  have overlapping nonzero support. The following proposition shows that our relaxation (5) is equivalent to the original problem (4) for many parameter settings of  $(\eta_1, \eta_2, \eta_3)$ . In cases where the supports of  $\mathbf{C}_p$  and  $\mathbf{C}_n$  overlap, we can also bound the magnitude of the overlapping entries (hence guaranteeing a close approximation of the solution to (4) from solutions to (5)). A proof is given in the appendix.

**Proposition 1.** Consider (5) with parameters  $\eta_1 > 0$  and  $\eta_2, \eta_3 \geq 0$ . Let  $(\mathbf{C}_p^*, \mathbf{C}_n^*, \mathbf{A}^*)$  be an optimal solution.

- 1) If  $\eta_1\eta_2 \leq \eta_3$ , then the solution of the relaxation (5) is the same as that of (4), when taking  $\mathbf{C} = \mathbf{C}_p - \mathbf{C}_n$ . In particular, the supports of  $\mathbf{C}_p^*$  and  $\mathbf{C}_n^*$  are disjoint.
- 2) If  $\eta_1\eta_2 > \eta_3$ , then the supports of  $\mathbf{C}_p^*$  and  $\mathbf{C}_n^*$  may overlap. At any index  $(i, j)$  for which  $(\mathbf{C}_p^*)_{ij} > 0$  and  $(\mathbf{C}_n^*)_{ij} > 0$ , it holds that

$$\max \left( (\mathbf{C}_p^*)_{ij}, (\mathbf{C}_n^*)_{ij} \right) < \frac{\eta_1\eta_2 - \eta_3}{\eta_1} \quad (6)$$

<sup>1</sup>Note that the  $l_1$  norm  $\|\mathbf{C}_p + \mathbf{C}_n\|_1$  can be replaced by the sum of the entries of  $\mathbf{C}_p + \mathbf{C}_n$  because of the nonnegativity constraints.

### 2.3. Sequential Approximation: A-DSSC

To see an alternative interpretation of the model in (4), note the following by expanding the second term of (4):

$$(4) = \min_{\mathbf{C}, \mathbf{A}} \frac{1}{2} \|\mathbf{X} - \mathbf{XC}\|_F^2 + \frac{\eta_1}{2} \|\mathbf{C}\|_F^2 + \eta_3 \|\mathbf{C}\|_1 - \langle \eta_1 |\mathbf{C}|, \eta_2 \mathbf{A} \rangle + \frac{\eta_1 \eta_2^2}{2} \|\mathbf{A}\|_F^2 \quad (7)$$

s.t.  $\mathbf{A} \in \Omega_n, \text{diag}(\mathbf{C}) = \mathbf{0}$

From this form, one can see that for an initialization of the affinity as  $\mathbf{A} = \mathbf{I}$ , the minimization w.r.t.  $\mathbf{C}$  takes the form of Elastic Net Subspace Clustering [43],

$$\min_{\mathbf{C}} \frac{1}{2} \|\mathbf{X} - \mathbf{XC}\|_F^2 + \frac{\eta_1}{2} \|\mathbf{C}\|_F^2 + \eta_3 \|\mathbf{C}\|_1 \quad (8)$$

s.t.  $\text{diag}(\mathbf{C}) = \mathbf{0}$

with  $\eta_1$  controlling the  $l_2$  regularization on  $\mathbf{C}$  and  $\eta_3$  controlling the  $l_1$  regularization. Likewise, for a fixed  $\mathbf{C}$ , one can observe that the above problem w.r.t.  $\mathbf{A}$  is a special case of a quadratically regularized optimal transport problem [2, 23]:

$$\min_{\mathbf{A}} \langle -\eta_1 |\mathbf{C}|, \eta_2 \mathbf{A} \rangle + \frac{\eta_1 \eta_2^2}{2} \|\mathbf{A}\|_F^2 \quad \text{s.t. } \mathbf{A} \in \Omega_n. \quad (9)$$

Thus, we see that  $\eta_2$  controls the regularization on  $\mathbf{A}$ , with a lower value of  $\eta_2$  encouraging sparse  $\mathbf{A}$  and higher  $\eta_2$  encouraging denser and more uniform  $\mathbf{A}$ . In particular, as  $\eta_2 \rightarrow 0$ , (9) approaches a linear assignment problem, which has permutation matrix solutions (i.e., maximally sparse solutions) [30, 14]. In contrast, as  $\eta_2 \rightarrow \infty$ , the optimal solution is densely connected and approaches the uniform matrix with all entries equal to  $\frac{1}{n}$ . These insights are used to develop our approximation model.

In particular, we consider an alternating minimization process to obtain approximate solutions for  $\mathbf{C}$  and  $\mathbf{A}$ , where we first initialize  $\mathbf{A}$  as  $\mathbf{A} = \mathbf{I}$  and solve (8) for  $\mathbf{C}$ . Then, holding  $\mathbf{C}$  fixed we solve (9) for  $\mathbf{A}$ . Taking the solution to this problem as the final affinity  $\mathbf{A}$ , we obtain our one-step approximation to J-DSSC, which we refer to as Approximate Doubly Stochastic Subspace Clustering (A-DSSC)<sup>2</sup>.

Besides being an approximation to the joint model (5), A-DSSC also has an interpretation as a postprocessing method for certain subspace clustering methods that can be expressed in the form of (8), such as SSC, EnSC, and LSR [8, 43, 25]. Instead of arbitrarily making choices about how to normalize/postprocess  $\mathbf{A}$  and form the normalized Laplacian, we instead take  $\mathbf{A}$  to be doubly stochastic; as discussed above, this provides a principled means of generating an affinity  $\mathbf{A}$  that is suitably normalized for spectral

<sup>2</sup>Note that additional alternating minimization steps can also be used as (7) is convex w.r.t.  $\mathbf{C}$  if  $\mathbf{A}$  is held fixed (for any feasible  $\mathbf{A}$ ) and vice-versa.

---

#### Algorithm 1 J-DSSC Outline.

---

**Input:** Data matrix  $\mathbf{X}$ , parameters  $\eta_1, \eta_2, \eta_3$   
**while** Not converged **do**  
    Update  $\mathbf{C}_p$  and  $\mathbf{C}_n$  by linearized ADMM steps  
    Update  $\mathbf{A}$ ,  $\mathbf{Y}$ , and  $\mathbf{Z}$  by minimization steps  
    Update dual variables by dual ascent steps  
**end while**  
Apply spectral clustering on Laplacian  $\mathbf{I} - \frac{1}{2}(\mathbf{A} + \mathbf{A}^\top)$   
**Output:** Clustering result

---



---

#### Algorithm 2 A-DSSC Outline.

---

**Input:** Data matrix  $\mathbf{X}$ , parameters  $\eta_1, \eta_2, \eta_3$   
Compute  $\mathbf{C}$  in (8) by an EnSC or LSR solver.  
Compute  $\alpha$  and  $\beta$  in (11) by L-BFGS.  
Recover  $\mathbf{A} = \frac{1}{\eta_2} \left[ |\mathbf{C}| - \alpha \mathbf{1}^\top - \mathbf{1} \beta^\top \right]_+$  as in (12).  
Apply spectral clustering on Laplacian  $\mathbf{I} - \frac{1}{2}(\mathbf{A} + \mathbf{A}^\top)$   
**Output:** Clustering result

---

clustering and invariant to the most common types of Laplacian normalization by solving a well-motivated convex optimization problem (9).

## 3. Optimization and Implementation

Here we outline the optimization procedures to compute our J-DSSC and A-DSSC models. Further algorithmic and implementation details are given in the appendix.

### 3.1. Joint Solution

In order to efficiently solve (5), we develop an algorithm in the style of linearized ADMM [26]. Specifically, we reparameterize the problem by introducing additional variables  $\mathbf{Y} = \mathbf{A}$  and  $\mathbf{Z} = \mathbf{X}[\mathbf{C}_p - \mathbf{C}_n]$ . This gives us the equivalent problem

$$\min_{\mathbf{C}_p, \mathbf{C}_n, \mathbf{A}, \mathbf{Y}, \mathbf{Z}} \frac{1}{2} \|\mathbf{X} - \mathbf{Z}\|_F^2 + \frac{\eta_1}{2} \left\| [\mathbf{C}_p + \mathbf{C}_n] - \eta_2 \mathbf{A} \right\|_F^2 + \eta_3 \|\mathbf{C}_p + \mathbf{C}_n\|_1 \quad (10)$$

s.t.  $\mathbf{A} \geq \mathbf{0}, \mathbf{C}_p, \mathbf{C}_n \in \mathbb{R}_{\geq 0, \text{diag}=0}^{n \times n}$ ,  
 $\mathbf{Y}^\top \mathbf{1} = \mathbf{Y} \mathbf{1} = \mathbf{1}, \mathbf{Y} = \mathbf{A}, \mathbf{Z} = \mathbf{X}[\mathbf{C}_p - \mathbf{C}_n]$

which we solve by a variant of linearized ADMM. In particular, we take linearized ADMM steps on  $\mathbf{C}_p$  and  $\mathbf{C}_n$ . Then we can efficiently minimize the associated augmented Lagrangian w.r.t.  $\mathbf{A}$ ,  $\mathbf{Y}$ , and  $\mathbf{Z}$ , by closed form solutions. Finally, we take dual ascent steps and repeat this process until convergence. The outline of the algorithm is given in Algorithm 1, with full details given in the appendix.

### 3.2. Approximation Solution

As previously suggested, the approximate model A-DSSC can be more efficient to solve than J-DSSC. First, the minimization over  $\mathbf{C}$  in (8) can be solved by certain scalable subspace clustering algorithms. In general, it is equivalent to Elastic Net Subspace Clustering (EnSC), for which scalable algorithms have been developed [43]. Likewise, in the special case of  $\eta_1 > 0, \eta_3 = 0$ , it is equivalent to Least Squares Regression (LSR) [25], which can be computed by a single  $n \times n$  linear system solve.

The regularized optimal transport problem (9) to solve for  $\mathbf{A}$  can be solved through the dual [2, 23], which gives an unconstrained problem over two vectors in  $\alpha, \beta \in \mathbb{R}^n$

$$\max_{\alpha, \beta} -\mathbf{1}^\top (\alpha + \beta) - \frac{1}{2\eta_2} \left\| \left[ |\mathbf{C}| - \alpha \mathbf{1}^\top - \mathbf{1} \beta^\top \right]_+ \right\|_F^2 \quad (11)$$

where  $[\cdot]_+$  denotes half-wave rectification, meaning that  $[\mathbf{x}]_+ = \max\{\mathbf{0}, \mathbf{x}\}$ , applied entry-wise. The optimal matrix  $\mathbf{A}$  is then recovered as:

$$\mathbf{A} = \frac{1}{\eta_2} \left[ |\mathbf{C}| - \alpha \mathbf{1}^\top - \mathbf{1} \beta^\top \right]_+ \quad (12)$$

We use L-BFGS [21] to solve for  $\alpha$  and  $\beta$  in (11). The outline of the algorithm to compute A-DSSC is given in Algorithm 2, with full details in the appendix.

### 3.3. Model Selection

Our method has three hyperparameters  $\eta_1, \eta_2, \eta_3$  to set. If we fix  $\mathbf{A}$ , the problem is simply EnSC [43]. This means that we may choose the parameters  $\eta_1$  and  $\eta_3$  in J-DSSC as is done in EnSC. As, noted in Section 2.2,  $\eta_2$  controls the sparsity of the final  $\mathbf{A}$ , with smaller  $\eta_2$  tending to give sparser  $\mathbf{A}$ . Thus, we choose  $\eta_2$  such that  $\mathbf{A}$  is within a desired average sparsity range. In addition, to avoid solutions that are too sparse, we can consider the number of connected components of the graph associated to the solution  $\mathbf{A}$ . If we want to obtain  $k$  clusters, we can adjust  $\eta_2$  so that the number of connected components is at most  $k$ . The parameters for A-DSSC can be selected in an analogous manner.

## 4. Experiments

In this section, we empirically study our models J-DSSC and A-DSSC. We show that our algorithm achieves state-of-the-art subspace clustering performance on a variety of real datasets with multiple performance metrics. Also, we investigate the behavior of our models on small datasets, showing various desirable properties of A-DSSC and J-DSSC.

### 4.1. Experimental Setup

**Algorithms.** We compare against several state-of-the-art subspace clustering algorithms, which are all affinity-based:

SSC [7, 8], EnSC [43], LSR [25], LRSC [35], TSC [13], SSC-OMP [44], S<sup>3</sup>COMP [4], and DSC-Net [17]. For these methods, we run the experiments on our own common framework, and we note that the results we obtain are very similar to those that have been reported previously in the literature on the same datasets for these methods. However, we do not have access to an implementation of S<sup>3</sup>COMP [4], so we report partial results from their paper, which we still include due to it being a recent well-performing model. Besides TSC, which uses an inner product similarity between data points, these methods all compute an affinity based on some self-expressive loss.

**Metrics.** As is standard in evaluations of clustering, we use clustering accuracy (ACC) [44] and normalized mutual information (NMI) [18] metrics, where we take the denominator in NMI to be the arithmetic average of the entropies. Also, we consider a subspace-preserving error (SPE), which is given by  $\frac{1}{n} \sum_{i=1}^n \sum_{j \notin \mathcal{S}_{y_i}} |\mathbf{A}_{ij}| / \|\mathbf{A}_i\|_1$ , where  $\mathcal{S}_{y_i}$  denotes the (subspace) cluster that point  $x_i$  belongs to, and  $\mathbf{A}_i$  is the  $i$ th column of  $\mathbf{A}$ . This measures the proportion of mass in the affinity that is erroneously given to points in different (subspace) clusters, and is often used in evaluation of subspace clustering algorithms [44, 33]. We report the sparsity of learned affinities by the average number of nonzeros per column (NNZ). Although sparse affinities are generally preferred, the sparsest affinity is not necessarily the best.

**Datasets.** We apply these algorithms for subspace clustering on the Extended Yale-B face dataset [9], Columbia Object Image Library (COIL-40 and COIL-100) [28], and UMIST face dataset [10]. We run experiments with the raw pixel data from the images and for the COIL and UMIST datasets also run separate experiments with features obtained from a scattering convolution network [3] reduced to dimension 500 by PCA [41]. This has been used in previous subspace clustering works [43, 4] to better embed the raw pixel data in a union of linear subspaces (whereas the raw pixel data does not necessarily have a union of subspaces structure). We do not use scattering transform features on the Yale-B dataset as it is already assumed to be well approximated by a union of linear subspaces [1]. Also, we do not evaluate DSC-Net on scattered features as the network architecture is only compatible with image data.

**Clustering setup.** For each baseline method we learn the  $\mathbf{C}$  from that method, form the affinity as  $\hat{\mathbf{A}} = (|\mathbf{C}| + |\mathbf{C}|^\top) / 2$ , take the normalized Laplacian  $\mathbf{L} = \mathbf{I} - \mathbf{D}^{-1/2} \hat{\mathbf{A}} \mathbf{D}^{-1/2}$  (where  $\mathbf{D} = \text{diag}(\hat{\mathbf{A}} \mathbf{1})$ ), and then apply spectral clustering with the specified number  $k$  of clusters [36]. For our DSSC methods, we form  $\hat{\mathbf{A}} = (\mathbf{A} + \mathbf{A}^\top) / 2$  and use  $\mathbf{L} = \mathbf{I} - \hat{\mathbf{A}}$  directly for spectral clustering (recall our affinity is invariant to Laplacian normalization). For the spectral clustering we take the  $k$  eigenvectors corresponding to the  $k$  smallest eigenvalues of  $\mathbf{L}$  as an embedding of the data. After normal-

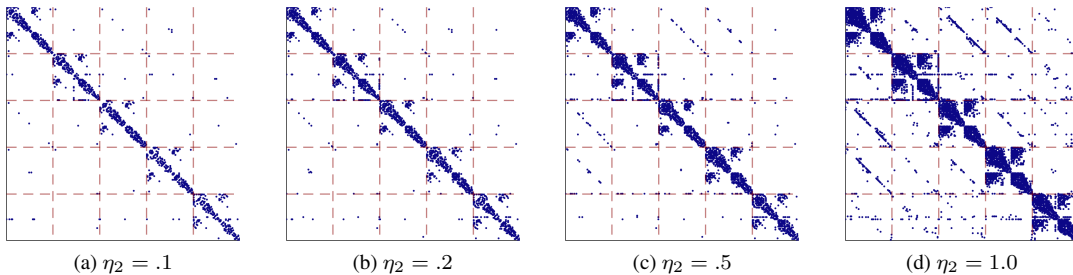


Figure 2. Affinity matrices  $\mathbf{A}$  learned by J-DSSC on the first five classes of Yale-B. We fix  $\eta_1 = .25$  and  $\eta_3 = 0$  (so there is no  $l_1$  regularization on  $\mathbf{C}$ ), while varying  $\eta_2$ . Red dashed lines mark the boundaries between classes. Dark blue points mark nonzero entries in  $\mathbf{A}$ . The learned affinity  $\mathbf{A}$  is sparser as  $\eta_2$  decreases, while it is more connected as  $\eta_2$  increases.

izing these embeddings to have unit  $l_2$  norm, we obtain 100 clusterings by random initializations of  $k$ -means clustering, compute the accuracy and NMI for each of these clusterings, then report the average accuracy and NMI as the final result. We emphasize that for each method we obtain a non-negative, symmetric affinity by a shared postprocessing of  $\mathbf{C}$  and/or  $\mathbf{A}$  instead of using different ad-hoc postprocessing methods that may confound the comparisons. Since DSC-Net is highly reliant on its ad-hoc postprocessing [11], we also report results with its postprocessing strategy applied (shown as DSC-Net-PP).

**Parameter choices.** As is often done in subspace clustering evaluation, we choose hyperparameters for each method by searching over some set of parameters and reporting the results that give the highest clustering accuracy. For the EnSC baseline we fix the  $l_1$  vs.  $l_2$  trade-off parameter  $\lambda = .5$  to avoid solutions too close to LSR or SSC. For DSC-Net, we use the suggested parameters in [17] where applicable, and search over hyperparameters for COIL-40. We give details on model hyperparameters in the appendix.

## 4.2. Results

Experimental results are reported in Table 1. On each dataset, one of our methods (J-DSSC and A-DSSC) achieves the highest clustering accuracy and NMI among all non-neural-network methods. In fact, on scattered data, DSSC achieves higher clustering accuracy and NMI than the neural method DSC-Net, even when allowing DSC-Net to use its ad-hoc postprocessing. DSC-Net with postprocessing does achieve better performance on Yale-B than our methods, though without postprocessing our models handily beat it, and we note that our method is a considerably simpler model than DSC-Net which requires training a neural network. Moreover, our models substantially outperform DSC-Net on both the raw pixel data and scattered embeddings of COIL-40 and COIL-100 — achieving perfect clusterings of COIL-40 and near-perfect clusterings of COIL-100. We also see that A-DSSC, which can be viewed as running SSC, EnSC or LSR followed by a principled

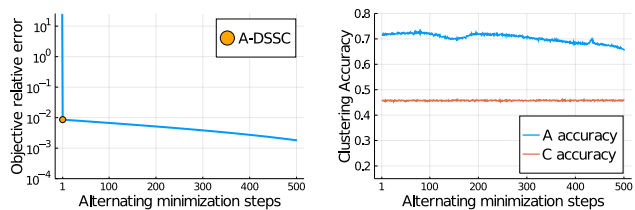


Figure 3. Objective value and clustering accuracy for different number of alternating minimization steps over  $\mathbf{C}$  in (8) then  $\mathbf{A}$  in (9) on the UMIST dataset. Our A-DSSC model is equivalent to 1 alternating minimization step. (Left) Shows relative error in the objective value compared to the true minimum. (Right) Shows clustering accuracy of using either  $\mathbf{A}$  or  $\mathbf{C}$  in spectral clustering.

doubly stochastic postprocessing, outperforms SSC, EnSC, and LSR across all datasets. This suggests that the doubly stochastic affinity matrices learned by our models are indeed effective as inputs into spectral clustering for the task of subspace clustering, and that our method can also potentially be combined with other subspace clustering methods as a principled postprocessing and normalization step.

Beyond just clustering accuracy, our models also learn affinity matrices with other desirable properties. The SPE of our models are usually the lowest among all methods, meaning that our learned affinities do not have significant misplaced mass connecting points from different subspaces. Likewise, the learned affinities tend to be rather sparse, with on average less than 15 nonzeros per column for the chosen parameters across all datasets. At the same time, the learned affinities have sufficient connectivity, as shown by the strong clustering accuracy.

## 4.3. Behavior of DSSC Models

Here, we explore the quality of our approximation A-DSSC by comparing the natural extension of this approximation to multiple steps of alternating minimization over  $\mathbf{C}$  in (8) and  $\mathbf{A}$  in (9). In particular, we note that additional alternating minimization steps do not bring a significant benefit over just a single alternating minimization iteration. Figure 3 displays the results of our A-DSSC model on

Table 1. Subspace clustering results on different datasets. ‘—’ indicates that we do not have results or the method cannot be run for the given entry. Best results with respect to ACC and NMI are **bolded**.

Dataset	Metric	Shallow Affinity-Based							Neural		Doubly Stochastic	
		SSC	EnSC	LSR	LRSC	TSC	SSC-OMP	S <sup>3</sup> COMP	DSC-Net	DSC-Net-PP	J-DSSC	A-DSSC
Yale-B	ACC	.654	.616	.659	.662	.514	.780	.874	.691	<b>.971</b>	.924	.917
	NMI	.734	.689	.743	.739	.629	.844	—	.746	<b>.961</b>	.952	.947
	SPE	.217	.249	.869	.875	.217	.179	.203	.881	.038	.080	.080
	NNZ	22.9	29.2	2413	2414	4.3	9.1	—	2414	22.1	14.5	14.4
COIL-40	ACC	.799	.649	.577	.567	.813	.411	—	.543	.751	.899	<b>.922</b>
	NMI	.940	.826	.761	.736	.916	.605	—	.743	.887	.963	<b>.967</b>
	SPE	.034	.103	.926	.877	.057	.025	—	.873	.105	.012	.008
	NNZ	3.1	31.5	2879	2880	4.5	2.9	—	2880	13.1	8.9	5.2
COIL-40 (Scattered)	ACC	.996	.838	.734	.753	.941	.489	—	—	—	<b>1.00</b>	<b>1.00</b>
	NMI	.998	.949	.868	.871	.981	.711	—	—	—	<b>1.00</b>	<b>1.00</b>
	SPE	.0002	.030	.787	.816	.004	.056	—	—	—	.00006	.00003
	NNZ	2.2	25.4	2879	2880	4.3	9.1	—	—	—	13.8	8.9
COIL-100	ACC	.704	.561	.492	.476	.723	.313	.789	.493	.635	.796	<b>.824</b>
	NMI	.919	.816	.753	.733	.904	.588	—	.752	.875	.943	<b>.946</b>
	SPE	.052	.163	.945	.946	.057	.052	.032	.958	.384	.049	.037
	NNZ	3.1	33.7	7199	7200	3.6	3.0	—	7200	44.7	9.9	5.8
COIL-100 (Scattered)	ACC	.954	.769	.642	.654	.915	.397	—	—	—	.961	<b>.984</b>
	NMI	.991	.929	.846	.850	.975	.671	—	—	—	.992	<b>.997</b>
	SPE	.002	.055	.891	.905	.009	.055	—	—	—	.004	.001
	NNZ	2.3	25.8	7199	7200	4.3	9.1	—	—	—	10.4	6.6
UMIST	ACC	.537	.499	.462	.494	.661	.509	—	.456	.708	<b>.732</b>	.725
	NMI	.718	.681	.645	.662	.829	.680	—	.611	.848	<b>.858</b>	.851
	SPE	.079	.154	.811	.824	.035	.091	—	.834	.393	.036	.034
	NNZ	4.9	19.2	574	575	3.7	2.9	—	575	23.2	5.1	4.8
UMIST (Scattered)	ACC	.704	.559	.524	.531	.714	.298	—	—	—	.873	<b>.888</b>
	NMI	.834	.747	.701	.711	.855	.416	—	—	—	<b>.939</b>	.935
	SPE	.038	.151	.758	.804	.030	.252	—	—	—	.020	.018
	NNZ	2.7	14.9	574	575	3.8	9.7	—	—	—	7.2	5.4

the UMIST face dataset [10] using the experimental setup described in Section 4.1. We see that a single alternating minimization step over  $\mathbf{C}$  then  $\mathbf{A}$ , which is equivalent to our A-DSSC model, already achieves most of the decrease in the objective (5) — giving a relative error of less than 1% compared to the global minimum obtained by the full J-DSSC solution. Moreover, the clustering accuracy is robust to additional alternating minimization steps beyond a single A-DSSC step — additional steps do not increase clustering accuracy from spectral clustering on  $\mathbf{A}$ . Also, spectral clustering on  $\mathbf{A}$  achieves much higher accuracy than spectral clustering on  $\mathbf{C}$ , thus showing the utility of the doubly stochastic model.

We also investigate the sparsity and connectivity of the affinity  $\mathbf{A}$  learned by our models. In Figure 2, we show sparsity plots of the learned matrices  $\mathbf{A}$  for J-DSSC models with varying  $\eta_2$  on the first five classes on the Extended Yale-B dataset [9]. The points are sorted by class, so intra-subspace connections are on the block diagonal, and inter-subspace connections are on the off-diagonal blocks. Here, it can be seen that the sparsity level of the recovered  $\mathbf{A}$  affinity is controlled by choice of the  $\eta_2$  parameter even when

there is no sparse regularization on  $\mathbf{C}$  (i.e.,  $\eta_3 = 0$ ), with the number of nonzeros increasing as  $\eta_2$  increases.

## 5. Conclusion

In this work, we propose a method to unify the self-expressive modeling of subspace clustering with the subsequent spectral clustering based on learning a doubly stochastic affinity matrix. We demonstrate experimentally that our methods achieve substantial improvements in subspace clustering accuracy over state-of-the-art models, without using any of the ad-hoc postprocessing steps that many other methods rely on. Our work further suggests many promising directions for future research by better merging the self-expressive modeling of subspace clustering with spectral clustering (or other graph clustering).

**Acknowledgements.** We thank Tianjiao Ding for helpful discussions. This work was partially supported by the Northrop Grumman Mission Systems Research in Applications for Learning Machines (REALM) initiative, the Johns Hopkins University Research Experience for Undergraduates in Computational Sensing and Medical Robotics (CSMR REU) program, NSF 1704458, and NSF 1934979.



## References

- [1] Ronen Basri and David W Jacobs. Lambertian reflectance and linear subspaces. *IEEE transactions on pattern analysis and machine intelligence*, 25(2):218–233, 2003. 6
- [2] Mathieu Blondel, Vivien Seguy, and Antoine Rolet. Smooth and sparse optimal transport. In *International Conference on Artificial Intelligence and Statistics*, pages 880–889, 2018. 3, 4, 5, 6
- [3] Joan Bruna and Stéphane Mallat. Invariant scattering convolution networks. *IEEE transactions on pattern analysis and machine intelligence*, 35(8):1872–1886, 2013. 6, 13
- [4] Ying Chen, Chun-Guang Li, and Chong You. Stochastic sparse subspace clustering. In *Proceedings of the IEEE/CVF Conference on Computer Vision and Pattern Recognition*, pages 4155–4164, 2020. 6
- [5] Ehsan Elhamifar, Guillermo Sapiro, and S Shankar Sastry. Dissimilarity-based sparse subset selection. *IEEE transactions on pattern analysis and machine intelligence*, 38(11):2182–2197, 2015. 3
- [6] Ehsan Elhamifar, Guillermo Sapiro, and René Vidal. Finding exemplars from pairwise dissimilarities via simultaneous sparse recovery. In *Advances in Neural Information Processing Systems*, pages 19–27, 2012. 3
- [7] Ehsan Elhamifar and René Vidal. Sparse subspace clustering. In *2009 IEEE Conference on Computer Vision and Pattern Recognition*, pages 2790–2797. IEEE, 2009. 1, 2, 6, 13
- [8] Ehsan Elhamifar and René Vidal. Sparse subspace clustering: Algorithm, theory, and applications. *IEEE transactions on pattern analysis and machine intelligence*, 35(11):2765–2781, 2013. 1, 2, 3, 4, 5, 6
- [9] Athinodoros S. Georghiadis, Peter N. Belhumeur, and David J. Kriegman. From few to many: Illumination cone models for face recognition under variable lighting and pose. *IEEE transactions on pattern analysis and machine intelligence*, 23(6):643–660, 2001. 6, 8, 13
- [10] Daniel B Graham and Nigel M Allinson. Characterising virtual eigensignatures for general purpose face recognition. In *Face Recognition*, pages 446–456. Springer, 1998. 6, 8, 13
- [11] Benjamin D. Haeffele, Chong You, and René Vidal. A critique of self-expressive deep subspace clustering. *arXiv preprint*, 2020. 3, 7
- [12] Amit Harlev, Charles R Johnson, and Derek Lim. The doubly stochastic single eigenvalue problem: A computational approach. *Experimental Mathematics*, pages 1–10, 2020. 2
- [13] Reinhard Heckel and Helmut Bölcskei. Robust subspace clustering via thresholding. *IEEE Transactions on Information Theory*, 61(11):6320–6342, 2015. 6, 13
- [14] Roger A Horn and Charles R Johnson. *Matrix analysis*. Cambridge university press, 2012. 2, 5
- [15] Eric Jankowski, Charles R Johnson, and Derek Lim. Spectra of convex hulls of matrix groups. *Linear Algebra and its Applications*, 2020. 2
- [16] Pan Ji, Mathieu Salzmann, and Hongdong Li. Efficient dense subspace clustering. In *IEEE Winter Conference on Applications of Computer Vision*, pages 461–468. IEEE, 2014. 3
- [17] Pan Ji, Tong Zhang, Hongdong Li, Mathieu Salzmann, and Ian Reid. Deep subspace clustering networks. In *Advances in Neural Information Processing Systems*, pages 24–33, 2017. 3, 6, 7, 14
- [18] Tarald O Kvalseth. Entropy and correlation: Some comments. *IEEE Transactions on Systems, Man, and Cybernetics*, 17(3):517–519, 1987. 6
- [19] Boris Landa, Ronald R Coifman, and Yuval Kluger. Doubly-stochastic normalization of the gaussian kernel is robust to heteroskedastic noise. *arXiv preprint arXiv:2006.00402*, 2020. 2, 3
- [20] Chun-Guang Li, Chong You, and René Vidal. Structured sparse subspace clustering: A joint affinity learning and subspace clustering framework. *IEEE Transactions on Image Processing*, 26(6):2988–3001, 2017. 3
- [21] Dong C Liu and Jorge Nocedal. On the limited memory bfgs method for large scale optimization. *Mathematical programming*, 45(1-3):503–528, 1989. 6
- [22] Guangcan Liu, Zhouchen Lin, Shuicheng Yan, Ju Sun, Yong Yu, and Yi Ma. Robust recovery of subspace structures by low-rank representation. *IEEE transactions on pattern analysis and machine intelligence*, 35(1):171–184, 2012. 3
- [23] Dirk A Lorenz, Paul Manns, and Christian Meyer. Quadratically regularized optimal transport. *Applied Mathematics & Optimization*, pages 1–31, 2019. 3, 5, 6
- [24] Canyi Lu, Jiashi Feng, Zhouchen Lin, Tao Mei, and Shuicheng Yan. Subspace clustering by block diagonal representation. *IEEE transactions on pattern analysis and machine intelligence*, 41(2):487–501, 2018. 3
- [25] Can-Yi Lu, Hai Min, Zhong-Qiu Zhao, Lin Zhu, De-Shuang Huang, and Shuicheng Yan. Robust and efficient subspace segmentation via least squares regression. In *European conference on computer vision*, pages 347–360. Springer, 2012. 1, 5, 6, 13
- [26] Shiqian Ma. Alternating proximal gradient method for convex minimization. *Journal of Scientific Computing*, 68(2):546–572, 2016. 3, 5
- [27] Behrooz Nasihatkon and Richard Hartley. Graph connectivity in sparse subspace clustering. In *CVPR 2011*, pages 2137–2144. IEEE, 2011. 2, 4
- [28] Sameer A Nene, Shree K Nayar, and Hiroshi Murase. Columbia object image library (coil-100). Technical report, Columbia University, 1996. 6, 13
- [29] Feiping Nie, Xiaoqian Wang, Michael I Jordan, and Heng Huang. The constrained laplacian rank algorithm for graph-based clustering. In *Thirtieth AAAI Conference on Artificial Intelligence*, 2016. 2, 3
- [30] Gabriel Peyré, Marco Cuturi, et al. Computational optimal transport: With applications to data science. *Foundations and Trends® in Machine Learning*, 11(5-6):355–607, 2019. 5
- [31] Nikitas Rontsis and Paul J. Goulart. Optimal approximation of doubly stochastic matrices. In *AISTATS*, 2020. 4
- [32] Jianbo Shi and Jitendra Malik. Normalized cuts and image segmentation. *IEEE Transactions on pattern analysis and machine intelligence*, 22(8):888–905, 2000. 1

- [33] Mahdi Soltanolkotabi, Emmanuel J Candes, et al. A geometric analysis of subspace clustering with outliers. *The Annals of Statistics*, 40(4):2195–2238, 2012. 6
- [34] René Vidal. Subspace clustering. *IEEE Signal Processing Magazine*, 28(2):52–68, 2011. 1
- [35] René Vidal and Paolo Favaro. Low rank subspace clustering (Irs). *Pattern Recognition Letters*, 43:47–61, 2014. 6, 13
- [36] Ulrike Von Luxburg. A tutorial on spectral clustering. *Statistics and computing*, 17(4):395–416, 2007. 1, 2, 3, 4, 6
- [37] Fei Wang, Ping Li, and Arnd Christian Konig. Learning a bi-stochastic data similarity matrix. In *2010 IEEE International Conference on Data Mining*, pages 551–560. IEEE, 2010. 2
- [38] Shusen Wang, Xiaotong Yuan, Tiansheng Yao, Shuicheng Yan, and Jialie Shen. Efficient subspace segmentation via quadratic programming. In *Twenty-Fifth AAAI Conference on Artificial Intelligence*, 2011. 3
- [39] Xiaoqian Wang, Feiping Nie, and Heng Huang. Structured doubly stochastic matrix for graph based clustering. In *Proceedings of the 22nd ACM SIGKDD International conference on Knowledge discovery and data mining*, pages 1245–1254, 2016. 2, 3, 12
- [40] Yining Wang, Yu-Xiang Wang, and Aarti Singh. Graph connectivity in noisy sparse subspace clustering. In *Artificial Intelligence and Statistics*, pages 538–546, 2016. 2, 4
- [41] Svante Wold, Kim Esbensen, and Paul Geladi. Principal component analysis. *Chemometrics and intelligent laboratory systems*, 2(1-3):37–52, 1987. 6
- [42] Jun Xu, Mengyang Yu, Deyu Meng, Wangpeng An, Ling Shao, Lei Zhang, and David Zhang. Simplex representation for subspace clustering. *arXiv preprint arXiv:1807.09930*, 2018. 3
- [43] Chong You, Chun-Guang Li, Daniel P Robinson, and René Vidal. Oracle based active set algorithm for scalable elastic net subspace clustering. In *Proceedings of the IEEE conference on computer vision and pattern recognition*, pages 3928–3937, 2016. 1, 2, 3, 4, 5, 6, 13
- [44] Chong You, Daniel Robinson, and René Vidal. Scalable sparse subspace clustering by orthogonal matching pursuit. In *Proceedings of the IEEE conference on computer vision and pattern recognition*, pages 3918–3927, 2016. 1, 2, 4, 6, 13
- [45] Ron Zass and Amnon Shashua. A unifying approach to hard and probabilistic clustering. In *Tenth IEEE International Conference on Computer Vision (ICCV'05) Volume 1*, volume 1, pages 294–301. IEEE, 2005. 2
- [46] Ron Zass and Amnon Shashua. Doubly stochastic normalization for spectral clustering. In *Advances in neural information processing systems*, pages 1569–1576, 2007. 2, 3, 4, 12
- [47] Pan Zhou, Yunqing Hou, and Jiashi Feng. Deep adversarial subspace clustering. In *Proceedings of the IEEE Conference on Computer Vision and Pattern Recognition*, pages 1596–1604, 2018. 14

# Appendices

## A. Derivation of A-DSSC Dual

Here, we give a derivation the dual (11) of the minimization over  $\mathbf{A}$  in A-DSSC. To see the derivation of the dual problem, first recall that the primal problem is:

$$\arg \min_{\mathbf{A}} \langle -\eta_1 |\mathbf{C}|, \eta_2 \mathbf{A} \rangle + \frac{\eta_1 \eta_2^2}{2} \|\mathbf{A}\|_F^2 \text{ s.t. } \mathbf{A} \in \Omega_n \quad (13)$$

$$= \arg \min_{\mathbf{A}} \langle -|\mathbf{C}|, \mathbf{A} \rangle + \frac{\eta_2}{2} \|\mathbf{A}\|_F^2 \text{ s.t. } \mathbf{A} \in \Omega_n. \quad (14)$$

Introducing Lagrange multipliers  $\alpha$  and  $\beta \in \mathbb{R}^n$  for the row and column sum constraints, we have the equivalent problem:

$$\min_{\mathbf{A} \geq 0} \max_{\alpha, \beta \in \mathbb{R}^n} \langle -|\mathbf{C}|, \mathbf{A} \rangle + \frac{\eta_2}{2} \|\mathbf{A}\|_F^2 + \langle \alpha, \mathbf{A} \mathbf{1} - \mathbf{1} \rangle + \langle \beta, \mathbf{A}^\top \mathbf{1} - \mathbf{1} \rangle \quad (15)$$

As the primal problem is convex and has a strictly feasible point, strong duality holds, so this is equivalent to:

$$\max_{\alpha, \beta \in \mathbb{R}^n} \min_{\mathbf{A} \geq 0} \langle -|\mathbf{C}|, \mathbf{A} \rangle + \frac{\eta_2}{2} \|\mathbf{A}\|_F^2 + \langle \alpha, \mathbf{A} \mathbf{1} - \mathbf{1} \rangle + \langle \beta, \mathbf{A}^\top \mathbf{1} - \mathbf{1} \rangle \quad (16)$$

$$= \max_{\alpha, \beta \in \mathbb{R}^n} -(\alpha + \beta)^\top \mathbf{1} + \min_{\mathbf{A} \geq 0} \langle -|\mathbf{C}|, \mathbf{A} \rangle + \frac{\eta_2}{2} \|\mathbf{A}\|_F^2 + \langle \alpha \mathbf{1}^\top + \mathbf{1} \beta^\top, \mathbf{A} \rangle \quad (17)$$

Letting  $\mathbf{K} = |\mathbf{C}| - \alpha \mathbf{1}^\top - \mathbf{1} \beta^\top$ , the inner minimization takes the form:

$$\min_{\mathbf{A} \geq 0} \langle -\mathbf{K}, \mathbf{A} \rangle + \frac{\eta_2}{2} \|\mathbf{A}\|_F^2 \quad (18)$$

$$= \eta_2 \min_{\mathbf{A} \geq 0} \langle -\frac{1}{\eta_2} \mathbf{K}, \mathbf{A} \rangle + \frac{1}{2} \|\mathbf{A}\|_F^2 \quad (19)$$

$$= -\frac{1}{2\eta_2} \|\mathbf{K}\|_F^2 + \eta_2 \min_{\mathbf{A} \geq 0} \frac{1}{2} \left\| \frac{1}{\eta_2} \mathbf{K} - \mathbf{A} \right\|_F^2 \quad (20)$$

$$= -\frac{1}{2\eta_2} \|\mathbf{K}\|_F^2 + \frac{1}{2\eta_2} \|\mathbf{K}_-\|_F^2 \quad (21)$$

$$= -\frac{1}{2\eta_2} \|\mathbf{K}_+\|_F^2 \quad (22)$$

Where  $[\mathbf{K}]_-$  is  $\min\{\mathbf{K}, \mathbf{0}\}$  taken elementwise. Thus, the final version of the dual is

$$\max_{\alpha, \beta \in \mathbb{R}^n} -(\alpha + \beta)^\top \mathbf{1} - \frac{1}{2\eta_2} \left\| \left[ |\mathbf{C}| - \alpha \mathbf{1}^\top - \mathbf{1} \beta^\top \right]_+ \right\|_F^2 \quad (23)$$

and the optimal value of  $\mathbf{A}$  is as given as

$$\mathbf{A} = \frac{1}{\eta_2} \left[ |\mathbf{C}| - \alpha \mathbf{1}^\top - \mathbf{1} \beta^\top \right]_+ \quad (24)$$

---

## Algorithm 3 J-DSSC

---

**Input:** Data matrix  $\mathbf{X}$ , parameters  $\eta_1, \eta_2, \eta_3$ , step sizes  $\rho$  and  $\tau$

**while** Not converged **do**

    Update  $\mathbf{C}_p$  and  $\mathbf{C}_n$  by linearized ADMM steps (28) to (31)

    Update  $\mathbf{A}$ ,  $\mathbf{Y}$ , and  $\mathbf{Z}$  by minimization steps (32) to (36)

    Update  $\lambda_1, \lambda_2, \Lambda_1$ , and  $\Lambda_2$  by dual ascent steps (37) to (40)

**end while**

    Apply spectral clustering on Laplacian  $\mathbf{I} - \frac{1}{2}(\mathbf{A} + \mathbf{A}^\top)$

**Output:** Clustering result

---

## B. Algorithm Details

### B.1. Linearized ADMM for J-DSSC

Here, we give details on the computation of J-DSSC. Consider the equivalent problem (10) with the added variables  $\mathbf{Y} = \mathbf{A}$  and  $\mathbf{Z} = \mathbf{X}[\mathbf{C}_p - \mathbf{C}_n]$ . The augmented Lagrangian takes the form:

$$\begin{aligned} \mathcal{L}(\mathbf{C}_p, \mathbf{C}_n, \mathbf{A}, \mathbf{Y}, \mathbf{Z}, \lambda, \Lambda) &= \frac{1}{2} \|\mathbf{X} - \mathbf{Z}\|_F^2 \\ &+ \frac{\eta_1}{2} \|\mathbf{C}_p + \mathbf{C}_n - \eta_2 \mathbf{A}\|_F^2 + \eta_3 \|\mathbf{C}_p + \mathbf{C}_n\|_1 \\ &+ \langle \lambda_1, \mathbf{Y}^\top \mathbf{1} - \mathbf{1} \rangle + \langle \lambda_2, \mathbf{Y} \mathbf{1} - \mathbf{1} \rangle + \langle \Lambda_1, \mathbf{Y} - \mathbf{A} \rangle \\ &+ \frac{\rho}{2} \|\mathbf{Y}^\top \mathbf{1} - \mathbf{1}\|_2^2 + \frac{\rho}{2} \|\mathbf{Y} \mathbf{1} - \mathbf{1}\|_2^2 + \frac{\rho}{2} \|\mathbf{Y} - \mathbf{A}\|_F^2 \\ &+ \langle \Lambda_2, \mathbf{Z} - \mathbf{X}[\mathbf{C}_p - \mathbf{C}_n] \rangle + \frac{\rho}{2} \|\mathbf{Z} - \mathbf{X}[\mathbf{C}_p - \mathbf{C}_n]\|_F^2 \\ &+ \mathcal{I}_{\geq 0}(\mathbf{A}) + \mathcal{I}_{\geq 0, \text{diag}=0}(\mathbf{C}_p) + \mathcal{I}_{\geq 0, \text{diag}=0}(\mathbf{C}_n) \end{aligned} \quad (25)$$

where  $\mathcal{I}_S$  is the indicator function for the set  $S$ , which takes values of 0 in  $S$  and  $\infty$  outside of  $S$ , and where  $\rho > 0$  is a chosen constant.

In each iteration, we take a linearized ADMM step in  $\mathbf{C}_p$  and  $\mathbf{C}_n$ , then alternately minimize over  $\mathbf{A}$ ,  $\mathbf{Y}$ , and  $\mathbf{Z}$ , and lastly take gradient ascent steps on each of the Lagrange multipliers. For a step size  $\tau > 0$ , the linearized ADMM step over  $\mathbf{C}_p$  takes the form of a gradient descent step on

$$\begin{aligned} h(\mathbf{C}_p) &= \langle \Lambda_2, \mathbf{Z} - \mathbf{X}[\mathbf{C}_p - \mathbf{C}_n] \rangle \\ &+ \frac{\rho}{2} \|\mathbf{Z} - \mathbf{X}[\mathbf{C}_p - \mathbf{C}_n]\|_F^2, \end{aligned} \quad (26)$$

followed by application of a proximal operator. Letting  $\mathbf{C}'_p$  be the intermediate value of  $\mathbf{C}_p$  after the gradient descent step,  $\mathbf{C}_p$  is updated as the solution to

$$\begin{aligned} \min_{\mathbf{C}_p} \frac{\eta_1}{2} \|\mathbf{C}_p + \mathbf{C}_n - \eta_2 \mathbf{A}\|_F^2 + \eta_3 \|\mathbf{C}_p + \mathbf{C}_n\|_1 \\ + \frac{1}{2\tau} \|\mathbf{C}'_p - \mathbf{C}_p\|_F^2 + \mathcal{I}_{\geq 0, \text{diag}=0}(\mathbf{C}_p) \end{aligned} \quad (27)$$

For a matrix  $\mathbf{E}$ , let  $[\mathbf{E}]_+$  be the half-wave rectification of  $\mathbf{E}$ , and let  $[\mathbf{E}]_{+, d=0}$  be the matrix  $\mathbf{E}$  with all negative entries and the diagonal set to zero. Then the linearized ADMM updates are given

as follows:

$$\mathbf{C}'_p \leftarrow \mathbf{C}_p - \tau \left( -\mathbf{X}^\top \mathbf{\Lambda}_2 + \rho \mathbf{X}^\top (\mathbf{X}[\mathbf{C}_p - \mathbf{C}_n] - \mathbf{Z}) \right) \quad (28)$$

$$\mathbf{C}_p \leftarrow \left[ \frac{1}{\eta_1 + \frac{1}{\tau}} \left( \frac{1}{\tau} \mathbf{C}'_p - \eta_1 \mathbf{C}_n + \eta_1 \eta_2 \mathbf{A} - \eta_3 \mathbf{1} \mathbf{1}^\top \right) \right]_{+,d=0} \quad (29)$$

$$\mathbf{C}'_n \leftarrow \mathbf{C}_n - \tau (\mathbf{X}^\top \mathbf{\Lambda}_2 - \rho \mathbf{X}^\top (\mathbf{X}[\mathbf{C}_p - \mathbf{C}_n] - \mathbf{Z})) \quad (30)$$

$$\mathbf{C}_n \leftarrow \left[ \frac{1}{\eta_1 + \frac{1}{\tau}} \left( \frac{1}{\tau} \mathbf{C}'_n - \eta_1 \mathbf{C}_p + \eta_1 \eta_2 \mathbf{A} - \eta_3 \mathbf{1} \mathbf{1}^\top \right) \right]_{+,d=0} \quad (31)$$

The sequential minimizations over  $\mathbf{A}$  then  $\mathbf{Y}$  then  $\mathbf{Z}$ , holding the other variables fixed and using the most recent value of each variable, take the form:

$$\mathbf{A} \leftarrow \left[ \frac{1}{\eta_1 \eta_2^2 + \rho} (\eta_1 \eta_2 [\mathbf{C}_p + \mathbf{C}_n] + \mathbf{\Lambda}_1 + \rho \mathbf{Y}) \right]_+ \quad (32)$$

$$\mathbf{Y} \leftarrow \frac{1}{\rho} \left[ \mathbf{V} - \frac{1}{n+1} \mathbf{P} \mathbf{V} \mathbf{1} \mathbf{1}^\top - \mathbf{1} \mathbf{1}^\top \mathbf{V} \frac{1}{n+1} \mathbf{P} \right] \quad (33)$$

$$\text{where } \mathbf{V} = \rho \mathbf{A} + 2\rho \mathbf{1} \mathbf{1}^\top - \mathbf{1} \lambda_1^\top - \lambda_2 \mathbf{1}^\top - \mathbf{\Lambda}_1 \quad (34)$$

$$\mathbf{P} = \mathbf{I} - \frac{1}{2n+1} \mathbf{1} \mathbf{1}^\top \quad (35)$$

$$\mathbf{Z} \leftarrow \frac{1}{1+\rho} (\mathbf{X} - \mathbf{\Lambda}_2 + \rho \mathbf{X}[\mathbf{C}_p - \mathbf{C}_n]) \quad (36)$$

The dual ascent steps on the Lagrange multipliers take the form:

$$\lambda_1 \leftarrow \lambda_1 + \rho (\mathbf{Y}^\top \mathbf{1} - 1) \quad (37)$$

$$\lambda_2 \leftarrow \lambda_2 + \rho (\mathbf{Y} \mathbf{1} - 1) \quad (38)$$

$$\mathbf{\Lambda}_1 \leftarrow \mathbf{\Lambda}_1 + \rho (\mathbf{Y} - \mathbf{A}) \quad (39)$$

$$\mathbf{\Lambda}_2 \leftarrow \mathbf{\Lambda}_2 + \rho (\mathbf{Z} - \mathbf{X}[\mathbf{C}_p - \mathbf{C}_n]) \quad (40)$$

Thus, the full J-DSSC algorithm is given in Algorithm 3.

To derive the minimization steps for a variable  $\mathbf{E}$  that is either  $\mathbf{C}_p$ ,  $\mathbf{C}_n$ ,  $\mathbf{A}$ , or  $\mathbf{Z}$ , we use the method of completing the square to change the corresponding minimization into one of the form  $\min_{\mathbf{E} \in S} \|\mathbf{E} - \mathbf{E}'\|_F^2$  for some feasible set  $S$  and some matrix  $\mathbf{E}'$ . For instance, in the case of  $\mathbf{C}_p$ , the set  $S$  is the set of  $n \times n$  nonnegative matrices with zero diagonal, and the solution is  $[\mathbf{E}']_{+,d=0}$ .

To minimize over  $\mathbf{Y}$ , we use different methods often used in dealing with row or column sum constraints [46, 39]. Define  $\mathbf{V} = \rho \mathbf{A} + 2\rho \mathbf{1} \mathbf{1}^\top - \mathbf{1} \lambda_1^\top - \lambda_2 \mathbf{1}^\top - \mathbf{\Lambda}_1$ . Setting the gradient of the augmented Lagrangian with respect to  $\mathbf{Y}$  equal to zero, we can show that

$$\rho \mathbf{Y} + \rho \mathbf{Y} \mathbf{1} \mathbf{1}^\top + \rho \mathbf{1} \mathbf{1}^\top \mathbf{Y} = \mathbf{V} \quad (41)$$

Multiplying both sides by  $\mathbf{1}$  on the right and noting that  $\mathbf{1}^\top \mathbf{1} = n$ , we have

$$\rho (\mathbf{I} + n \mathbf{I} + \mathbf{1} \mathbf{1}^\top) \mathbf{Y} \mathbf{1} = \mathbf{V} \mathbf{1} \quad (42)$$

$$\rho \mathbf{Y} \mathbf{1} = (\mathbf{I} + n \mathbf{I} + \mathbf{1} \mathbf{1}^\top)^{-1} \mathbf{V} \mathbf{1} \quad (43)$$

Likewise, multiplying by  $\mathbf{1}^\top$  on the left gives that

$$\rho \mathbf{1}^\top \mathbf{Y} = \mathbf{1}^\top \mathbf{V} (\mathbf{I} + n \mathbf{I} + \mathbf{1} \mathbf{1}^\top)^{-1} \quad (44)$$

We use the Woodbury matrix identity to compute the inverse

$$(\mathbf{I} + n \mathbf{I} + \mathbf{1} \mathbf{1}^\top)^{-1} = \frac{1}{n+1} \left( \mathbf{I} - \frac{1}{2n+1} \mathbf{1} \mathbf{1}^\top \right). \quad (45)$$

We define  $\mathbf{P} = \mathbf{I} - \frac{1}{2n+1} \mathbf{1} \mathbf{1}^\top$ , so the inverse is  $\frac{1}{n+1} \mathbf{P}$ . Thus, using both (43) and (44) in the left hand side of (41) gives that

$$\rho \mathbf{Y} + \frac{1}{n+1} \mathbf{P} \mathbf{V} \mathbf{1} \mathbf{1}^\top + \mathbf{1} \mathbf{1}^\top \mathbf{V} \frac{1}{n+1} \mathbf{P} = \mathbf{V} \quad (46)$$

and thus the minimizing  $\mathbf{Y}$  is given as

$$\mathbf{Y} = \frac{1}{\rho} \left[ \mathbf{V} - \frac{1}{n+1} \mathbf{P} \mathbf{V} \mathbf{1} \mathbf{1}^\top - \mathbf{1} \mathbf{1}^\top \mathbf{V} \frac{1}{n+1} \mathbf{P} \right]. \quad (47)$$

## B.2. Implementation Details

We implement our methods in the Julia programming language. For the J-DSSC algorithm, we take the step sizes to be  $\rho = .5$  and  $\tau = .0001$  for our experiments.

**Complexity Analysis.** Let  $\mathbf{X} \in \mathbb{R}^{d \times n}$ , so there are  $n$  data points in  $\mathbb{R}^d$ . For J-DSSC, each update on  $\mathbf{C}_p$  and  $\mathbf{C}_n$  takes  $\mathcal{O}(dn^2)$  operations due to matrix multiplications. Each update on  $\mathbf{A}$  and  $\mathbf{Y}$  takes  $\mathcal{O}(n^2)$  operations, while each update on  $\mathbf{Z}$  takes  $\mathcal{O}(dn^2)$ . The dual ascent steps also take  $\mathcal{O}(dn^2)$  operations in total. Thus, each iteration of the linearized ADMM part takes  $\mathcal{O}(dn^2)$ . We note in particular that J-DSSC does not require the solution of any linear systems or any singular value decompositions, while many other subspace clustering methods do. For A-DSSC, solving for  $\mathbf{C}$  is done by some efficient EnSC, SSC, or LSR solver. The quadratically regularized optimal transport step takes  $\mathcal{O}(n^2)$  operations per objective function evaluation and gradient evaluation.

The spectral clustering step requires a partial eigendecomposition of  $\mathbf{I} - \frac{1}{2}(\mathbf{A} + \mathbf{A}^\top)$ , although we note that in practice the  $\mathbf{A}$  that is learned tends to be sparse for the parameter settings that we choose, so we can leverage sparse eigendecomposition algorithms to compute the  $k$  eigenvectors corresponding to the smallest eigenvalues. Recall that all subspace clustering methods that use spectral clustering (which is the majority of methods) require computing an eigendecomposition of equivalent size, though not all subspace clustering affinities can leverage sparse eigendecomposition methods.

## C. Proof of Proposition 1

*Proof.* Suppose that there is an index  $(i, j)$  such that

$$a = (\mathbf{C}'_p)_{ij} > 0, \quad b = (\mathbf{C}'_n)_{ij} > 0. \quad (48)$$

Define matrices  $\mathbf{C}'_p$  and  $\mathbf{C}'_n$  such that  $\mathbf{C}'_p$  matches  $\mathbf{C}^*_p$  at every index but  $(i, j)$  and similarly for  $\mathbf{C}'_n$ . At index  $(i, j)$ , we define

$$(\mathbf{C}'_p)_{ij} = \max(a - b, 0), \quad (\mathbf{C}'_n)_{ij} = \max(b - a, 0) \quad (49)$$

We consider the value of the expanded J-DSSC objective (7) at  $(\mathbf{C}'_p, \mathbf{C}'_n, \mathbf{A}^*)$  compared to the value at  $(\mathbf{C}^*_p, \mathbf{C}^*_n, \mathbf{A}^*)$ . Note that  $\mathbf{C}'_p - \mathbf{C}'_n = \mathbf{C}^*_p - \mathbf{C}^*_n$ . Thus, there are only three summands in the objective that are different between the two groups of variables.

Suppose  $a \geq b$ . The differences are computed as:

$$\begin{aligned} & \frac{\eta_1}{2} \left\| \mathbf{C}'_p + \mathbf{C}'_n \right\|_F^2 - \frac{\eta_1}{2} \left\| \mathbf{C}^*_p + \mathbf{C}^*_n \right\|_F^2 \\ &= \frac{\eta_1}{2} \left( (a-b)^2 - (a+b)^2 \right) \\ &= -2\eta_1 ab \end{aligned} \quad (50)$$

$$\begin{aligned} & -\eta_1 \langle [\mathbf{C}'_p + \mathbf{C}'_n], \eta_2 \mathbf{A}^* \rangle + \eta_1 \langle [\mathbf{C}^*_p + \mathbf{C}^*_n], \eta_2 \mathbf{A}^* \rangle \\ &= \eta_1 \eta_2 (\mathbf{A}^*)_{ij} (-|a-b| + (a+b)) \\ &= 2\eta_1 \eta_2 (\mathbf{A}^*)_{ij} b \end{aligned} \quad (51)$$

$$\begin{aligned} & \eta_3 \left\| \mathbf{C}'_p + \mathbf{C}'_n \right\|_1 - \eta_3 \left\| \mathbf{C}^*_p + \mathbf{C}^*_n \right\|_1 \\ &= \eta_3 (|a-b| - (a+b)) \\ &= -2\eta_3 b \end{aligned} \quad (52)$$

Now, we bound the difference between the objective functions for the two variables:

$$\begin{aligned} 0 &< -2\eta_1 ab + 2\eta_1 \eta_2 (\mathbf{A}^*)_{ij} b - 2\eta_3 b \\ &\leq -2\eta_1 ab + 2\eta_1 \eta_2 b - 2\eta_3 b \end{aligned}$$

where the first bound is due to  $(\mathbf{C}^*_p, \mathbf{C}^*_n, \mathbf{A}^*)$  being the optimal solution, and the upper bound is due to  $(\mathbf{A}^*)_{ij} \leq 1$ . From these bounds, we have that

$$b \leq a < \frac{\eta_1 \eta_2 - \eta_3}{\eta_1}. \quad (53)$$

Where we recall that we assumed  $b \leq a$ . A similar upper bound holds with  $b$  taking the place of  $a$  in the case where  $b > a$ . Now, note that  $a > 0$  means that  $\eta_1 \eta_2 > \eta_3$ , thus proving 1) through the contrapositive. This bound clearly gives the one in (6), so we have also proven 2).  $\square$

## D. Data Details

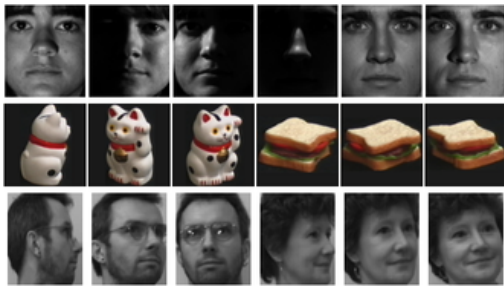


Figure 4. Sample images from Extended Yale-B (top row), COIL-100 (middle row), and UMIST (bottom row).

Table 2. Statistics and properties of datasets.

Dataset	# Images ( $n$ )	Dimension	# Classes
Yale-B	2414	$48 \times 42$	38
COIL-40	2880	$32 \times 32$	40
COIL-100	7200	$32 \times 32$	100
UMIST	575	$32 \times 32$	20

For our experiments, we run subspace clustering on the Extended Yale-B face dataset [9], Columbia Object Image Library (COIL-40 and COIL-100) [28], and UMIST face dataset [10]. Sample images from these datasets are shown in Figure 4. Basic statistics and properties of these datasets are given in Table 2.

The scattered data is computed as in [43, 44], by using a scattering convolution network [3] to compute a feature vector of 3,472 dimensions for UMIST and  $3 \cdot 3,472 = 10,416$  dimensions for COIL (since there are three color channels), then projecting to 500 dimensions by PCA. For both pixel data and scattered data, we normalize each data point to have unit  $l_2$  norm for all experiments, noting that scaling a data point does not change its subspace membership.

For Yale-B, we remove the 18 images labeled as corrupted in the dataset, leaving 2414 images for our experiments. Adding the corrupted images back in does not appear to qualitatively change our results. We resize Yale-B to size  $48 \times 42$ . The COIL images and UMIST images are resized to size  $32 \times 32$ .

## E. Parameter Settings

Table 3. Parameter settings for J-DSSC and A-DSSC.

Dataset	J-DSSC			A-DSSC		
	$\eta_1$	$\eta_2$	$\eta_3$	$\eta_1$	$\eta_2$	$\eta_3$
Yale-B	.25	.2	0	.5	.1	0
COIL-40	25	.01	.1	25	.001	0
COIL-40 (Scattered)	.25	.2	0	50	.001	0
COIL-100	25	.01	.1	50	.0005	0
COIL-100 (Scattered)	.25	.1	0	.1	.025	0
UMIST	1	.05	0	.5	.05	0
UMIST (Scattered)	.01	.2	0	.5	.01	0

Table 4. Parameters searched over for different methods.

Method	Parameters and Variant
SSC [7]	$\gamma \in \{1, 5, 10, 25, 50, 100, 1000\}$ , noisy data variant
EnSC [43]	$\gamma \in \{.1, 1, 5, 10, 50, 100, 200\}$ , $\lambda = .5$
LSR [25]	$\lambda \in \{.01, .1, .5, 1, 10, 50, 100\}$ , $\text{diag}(\mathbf{C}) = \mathbf{0}$ variant
LRSC [35]	$\tau \in \{.1, 1, 10, 50, 100, 500, 1000\}$ , $\alpha = \tau/2$ , noisy data and relaxed constraint variant
TSC [13]	$q \in \{2, 3, \dots, 14, 15\}$
SSC-OMP [44]	$k_{\max} \in \{2, 3, \dots, 14, 15\}$
J-DSSC (Ours)	$\eta_1 \in \{.01, .25, 1, 25\}$ , $\eta_2 \in \{.01, .05, .1, .2\}$ , $\eta_3 \in \{0, .1\}$
A-DSSC (Ours)	$\eta_1 \in \{.1, 1, 10, 25, 50\}$ , $\eta_2 \in \{.0005, .001, .01, .025, .05, .1\}$ , $\eta_3 = 0$

Here, we give parameter settings for the experiments in the paper. The chosen parameter settings for our DSSC models are given

in Table 3. We note that the experiments on UMIST to explore the objective value over iterations of alternating minimization in Figure 3 use the same parameter settings as in this table.

The parameters searched over for the non-neural methods are given in Table 4.

For DSC-Net, we use the hyperparameters and pre-trained autoencoders as in their original paper [17] for Yale-B and COIL-100. For DSC-Net on UMIST, we take a similar architecture to that of [47], with encoder kernel sizes of  $5 \times 5, 3 \times 3, 3 \times 3$ , as well as 15, 10, 5 channels per each layer. The regularization parameters are set as  $\lambda_1 = 1$  and  $\lambda_2 = .2$ . The DSC-Net post-processing on UMIST is taken to be similar to that used for ORL. For COIL-40, we use one encoder layer of kernel size  $3 \times 3$ , 20 channels, and regularization parameters  $\lambda_1 = 1, \lambda_2 = 100$ ; we also use the same postprocessing that is used for COIL-100.